PHOSPHO1 is essential for mechanically competent mineralization and the avoidance of spontaneous fractures

Published in final edited form as:
Bone. 2011 May 1; 48(5): 1066–1074. doi:10.1016/j.bone.2011.01.010.

PHOSPHO1 is essential for mechanically competent mineralization and the avoidance of spontaneous fractures

Carmen Huesa[1], **Manisha C. Yadav**[2], **Mikko A.J. Finnilä**[3,4], **Simon R. Goodyear**[5], **Simon P. Robins**[6], **K. Elizabeth Tanner**[3], **Richard M. Aspden**[5], **José Luis Millán**[2], and **Colin Farquharson**[1]

Carmen Huesa: carmen.huesa@roslin.ed.ac.uk; Manisha C. Yadav: myadav@sanfordburnham.org; Mikko A.J. Finnilä: mikko.finnila@oulu.fi; Simon R. Goodyear: s.goodyear@abdn.ac.uk; Simon P. Robins: s.robins@abdn.ac.uk; K. Elizabeth Tanner: K.Tanner@civil.gla.ac.uk; Richard M. Aspden: r.aspden@abdn.ac.uk; José Luis Millán: millan@sanfordburnham.org; Colin Farquharson: colin.farquharson@roslin.ed.ac.uk

[1]Bone Biology Group, The Roslin Institute and Royal (Dick) School of Veterinary Studies, University of Edinburgh, Edinburgh, UK. [2]Sanford Children's Health Research Center, Sanford-Burnham Medical Research institute, La Jolla, CA, USA. [3]Department of Mechanical Engineering, Materials, University of Glasgow, Glasgow, UK. [4]Department of Medical Technology, Institute of Biomedicine, University of Oulu, Oulu, Finland. [5]Institute of Medical Sciences, Foresterhill, University of Aberdeen, Aberdeen, UK. [6]Matrix Biochemistry Group, Rowett Research Institute of Health and Nutrition, University of Aberdeen, Aberdeen, UK.

Abstract

Phosphatases are essential for the mineralization of the extracellular matrix within the skeleton. Their precise identities and functions however remain unclear. PHOSPHO1 is a phosphoethanolamine/phosphocholine phosphatase involved in the generation of inorganic phosphate for bone mineralization. It is highly expressed at sites of mineralization in bone and cartilage. The bones of *Phospho1*$^{-/-}$ mice are hypomineralized, bowed and present with spontaneous greenstick fractures at birth. In this study we show that PHOSPHO1 is essential for mechanically competent mineralization that is able to withstand habitual load. Long bones from *Phospho1*$^{-/-}$ mice did not fracture during 3- point bending but deformed plastically. With dynamic loading nanoindentation the elastic modulus and hardness of *Phospho1*$^{-/-}$ tibiae were significantly lower than wild-type tibia. Raman microscopy revealed significantly lower mineral:matrix ratios and lower carbonate substitutions in *Phospho1*$^{-/-}$ tibia. The altered dihydroxylysinonorleucine/hydroxyllysinonorleucine and pyridoline/deoxypyridinoline collagen crosslink ratios indicated possible changes in lysyl hydroxylase-1 activity and/or bone mineralization status. The bone formation and resorption markers, N-terminal propeptide and C-terminal telopeptide of Type I collagen, were both increased in *Phospho1*$^{-/-}$ mice and this we associated with increased bone remodelling during fracture repair or an attempt to remodel a mechanically competent bone capable of withstanding physiological load. In summary these data

Corresponding Author: Dr. Carmen Huesa, Bone Biology Group, The Roslin Institute and Royal (Dick) School of Veterinary Studies, University of Edinburgh, UK. Tel: 00 44 (0)131 527 4228; Fax: 00 44 (0)131 440 0434; carmen.huesa@roslin.ed.ac.uk.

Conflict of Interest
All authors report no conflict of interest.

indicate that *Phospho1*$^{-/-}$ bones are hypomineralized and, consequently, are softer and more flexible. An inability to withstand physiological loading may explain the deformations noted. We hypothesize that this phenotype is due to the reduced availability of inorganic phosphate to form hydroxyapatite during mineralization, creating an undermineralized yet active bone.

Keywords

Phospho1; biomineralization; mechanical and material properties; bone quality; hypomineralization

1 Introduction

During bone growth, formation and development, the mineralization of the extracellular matrix (ECM) of both chondrocytes and osteoblasts involves the deposition of crystalline hydroxyapatite (HA) within the interior of membrane-limited matrix-vesicles (MVs) [1–3]. This process is instigated by the accumulation of Ca^{2+} and inorganic phosphate (Pi) within MVs resulting in the formation of HA crystals. This initial phase is followed by MV membrane rupture/breakdown and the modulation of ECM composition to further promote propagation of HA outside of the MVs [1–3]. ECM mineralization is a highly regulated process and chondrocytes, osteoblasts and their derived MVs accomplish this by expressing Pi-transporters for Pi uptake [4–5], annexin V for Ca^{2+} influx [6] and regulators of inorganic pyrophosphate (PPi) metabolism [7]. Extracellular PPi is a recognized potent mineralization inhibitor in biological fluids [8] and its concentration is regulated by tissue-nonspecific alkaline phosphatase (TNAP) which hydrolyzes PPi in the ECM to establish a Pi/PPi ratio permissive for the initial formation of HA crystals within MVs [9–12]. Also, nucleotide pyrophosphatase phosphodiesterase 1 (NPP1) ectoplasmically generates PPi from nucleoside triphosphates [13], and the multiple-pass transmembrane protein ANK mediates intracellular to extracellular channelling of PPi [14–15].

In addition to its PPi hydrolase activity, TNAP also has recognized ATPase activity [16] and disruption of PPi and/or ATP hydrolysis may contribute to hypophosphatasia (HPP), an inborn error of metabolism resulting in rickets and osteomalacia [17]. Mice deficient in TNAP function (*Akp2*$^{-/-}$) phenocopy infantile HPP *i.e.* their skeleton at birth is mineralized normally but hypomineralization rapidly ensues within 1 – 2 weeks of postnatal life before death at postnatal day 20 [18–19]. The failure of bone to mineralize properly after birth in *Akp2*$^{-/-}$ mice has been associated with PPi accumulating within the ECM and blocking the propagation of HA in the ECM beyond the confines of the MV membrane [20–21]. An explanation as to why the skeleton of *Akp2*$^{-/-}$ mice are normally mineralized at birth has focussed on the existence of other phosphatases responsible for MV-mediated ECM mineralization and PHOSPHO1 which was identified 10 years ago is a strong candidate for this missing phosphatase. Since its discovery and characterization [16,22–27] we have proposed that PHOSPHO1 is, in part, responsible for Pi accumulation (and HA formation) within the MV through its phosphohydrolase activity towards the membrane phospholipids, phosphoethanolamine and phosphocholine [26,28]. Consequently, due to its cytosolic localization and its known presence and activity within MVs [24–25], PHOSPHO1 is likely to be partly responsible for the intravesicular HA formation noted in MVs derived from HPP and *Akp2*$^{-/-}$ chondrocytes and osteoblasts [20–21]. The critical importance of PHOSPHO1 for skeletal mineralization has been recently suggested by the use of small molecule compounds to inhibit PHOSPHO1 activity in MVs and developing embryonic chick limbs *in vivo* [25,27]. Definitive evidence for a mineralization role of PHOSPHO1 was obtained in a comparison of the bone phenotype of *Phospho1*$^{-/-}$, *Akp2*$^{-/-}$ and *Phospho1*$^{-/-}$*; Akp2*$^{-/-}$ double knockout mice [29]. The *Akp2*$^{-/-}$ and *Phospho1*$^{-/-}$ mice are both characterized by

lower skeletal mineralization whereas the double ablation of PHOSPHO1 and TNAP leads to the complete absence of skeletal mineralization. These data are strongly supportive of independent, non-redundant mechanisms of action of both phosphatases in the mineralization process [18,29].

Whilst the functional importance of PHOSPHO1 in regulating skeletal mineralization has now been clearly demonstrated [29] it is still unclear as to how PHOSPHO1 fully contributes to the maintenance of bone quality and ultimately, bone strength. Our aim was to analyse the role of PHOSPHO1 during this developmental phase and not at adulthood where any alterations noted in skeletal integrity may be secondary and a consequence of earlier developmental cues. Such information is essential if we are to understand fully the physiological role of PHOSPHO1 in the maintenance of skeletal integrity and explain the pathological long bone bowing and spontaneous greenstick fractures noted in *Phospho1*$^{-/-}$ mice [29]. In this paper we conclusively demonstrate that PHOSPHO1 is essential for the proper formation of mechanically competent bones able to withstand habitual load.

2 Materials and Methods

2.1 Mice and Tissues

Phospho1-R74X-null mutant (*Phospho1*$^{-/-}$) mice were generated by N-ethyl-N-nitrosourea mutagenesis (ENU) as previously described [29]. We chose to study mice at one month of age as the skeletal abnormalities previously described by us [29] present immediately after birth and during juvenile development. For the study of material and mechanical properties and collagen cross-link analysis, 7 wild-type (WT) and 9 *Phospho1*$^{-/-}$ 30-day old male mice were euthanized and their right tibia and right femur were removed and stored in distilled H_2O at −20°C. The left tibia was removed and fixed in 4% paraformaldehyde (PFA) for static histomorphometric analysis. In further studies, dynamic histomorphometry was completed in calcein labelled male mice (8 WT and 8 *Phospho1*$^{-/-}$). Mice were injected i.p. with calcein (10 mg/kg in 1.4% w/v $NaHCO_3$) at 19-days and then again at 29 days of age. Mice were sacrificed at 30 days of age and the left tibia from each mouse was dissected and processed as described by Rawlinson *et al.* [30] Blood was collected by cardiac puncture from 30-day old male mice (14 WT and 16 *Phospho1*$^{-/-}$) and serum separated using serum-clotting-activator tubes (Starstedt Ltd., UK). All animal studies were approved by the Institutional Animal Users' Committees of the Sanford-Burnham Medical Research Institute, La Jolla, CA and The Roslin Institute, UK.

2.2 3-point bending for the determination of bone stiffness and breaking strength

An Instron 5564 materials testing machine (Instron, High Wycombe, UK) fitted with a 2 kN load cell was used to determine bone stiffness and breaking strength [31]. The span was fixed at 5.12 mm for femora and at 6.95 mm for tibiae. The cross-head was lowered at 1 mm/min and data were recorded after every 0.2 N change in load and every 0.1 mm change in deflection. Each bone was tested to fracture. Failure and fracture points were identified from the load-extension curve as the point of maximum load and where the load rapidly decreased to zero, respectively. The maximum stiffness was defined as the maximum gradient of the rising portion of this curve, and the yield point, the point at which the gradient reduced to 95% of this value. Both values were calculated from a polynomial curve fitted to the rising region of the load-extension curve in Mathcad (Mathsoft Engineering and Education Inc., Cambridge, MA, USA).

2.3 Raman microscopy

Raman microscopy and nanoindentation (see below) were conducted on cortical bone fragments of both tibia and femur after the completion of the 3-point bending analysis. A ~2

mm transverse section of the diaphyses were analyzed by Raman microscopy as previously described [32]. The collected data were processed as described by Goodyear *et al.* [32] Intensities of bands representing mineral (phosphate v_4), matrix (amide III), carbonate and acid phosphate (HPO_4^{-}) were measured and ratios calculated. The full width at half maximum height of the phosphate symmetric stretching vibration (v_1) was measured to estimate the crystallinity of the bone mineral [33].

2.4 Nanoindentation

Bone slices were embedded in epoxy resin (EPO-SET, MetPrep Ltd, Coventry, UK) for nanoindentation. The blocks were then grounded using sand paper successively decreasing grid size closer the diaphyseal cross section was from surface. Once the whole cross-section was visible at the surface final polishing was done with 5 μm and then 1 μm diamond suspension and finalized with 0.05 μm γ-alumina slurry (MetPrep Ltd, Coventry, UK). Nanoindentations were performed using a G200 nanoindenter (Agilent Technologies) fitted with a Berkovich shaped diamond tip having a Poisson ratio of 0.07 and elastic modulus of 114 GPa. The indenter was controlled with Testworks 4 version 4.10 (MTS System Corporation) to produce 60 indentations using both quasistatic and dynamic loading schemes [34]. Indentations for tibiae were done in the anterior-medial aspect of the transverse diaphyseal bone, while indentations in the femur were done on an anterior section. Both regions corresponded to areas previously analyzed by Raman microscopy. All indentations were inspected with a optical microscope (Nikon Eclipse ME600) equipped with Nomarski optics to remove indentations falling into a pore [35]. Data were processed as previously described [34,36].

2.5 Biochemical analysis of bone

Representative diaphysial samples of the tibia and femur without cartilaginous remnants were equilibrated in 0.14M NaCl – 50 mM sodium phosphate, pH 7.5, reduced with potassium borohydride and finally freeze dried after extensive washing. Weighed samples were hydrolyzed in 5.7M HCl at 107°C for 20 h. After removal of HCl by evaporation *in vacuo* the samples were placed in 1.0 ml water. For measurements of collagen cross-links, preliminary fractionation of the hydrolysates was performed by partition chromatography [37] and the components were determined by liquid chromatography/mass spectrometry using methods similar to those described by Gineyts *et al.* [38] except that a tandem instrument (QTRAP® API 4000, Applied Biosystems, Warrington, UK) was used with specific transitions for each cross-link component. The mature cross-links, pyridinoline (PYD) and deoxypyridinoline (DPD), and reduced forms of the immature bonds, dihydroxylysinonorleucine (DHLNL) and hydroxylysinonorleucine (HLNL), were quantified by reference to standard curves prepared with authentic components. Hydroxyproline was measured by colorimetric assay according to Firschein and Shill [39], and the collagen content of bone was calculated assuming each collagen molecule contains 300 residues of hydroxyproline. Calcium was measured using the Jaffe method on a Kone autoanalyzer and the results expressed in relation to the dry weight of bone and its collagen content.

2.6 Histomorphometry and dynamic histomorphometry

For static histomorphometry, tibia were fixed in 4% PFA for 24 h, decalcified in 10% EDTA at 4°C for 21 days, dehydrated using alcohols and embedded in wax using standard procedures. Longitudinal wax sections (10μm) through the diaphysis and epiphysis were cut onto ‘Superfrost’ slides (VWR International Ltd, Lutterworth, UK). After dewaxing in xylene and rehydration in a descending series of alcohols the sections were stained with 1 % toluidine blue to visualize osteoblasts and reacted for tartrate resistant acid phosphatase (TRAP) activity using standard methods to visualize osteoclasts. Sections were examined

using a Leitz DMRB microscope and images captured with a Leica DFC300 FX camera at 20X magnification. Images were analyzed using ImageJ and osteoclast number/bone perimeter (Noc/BPm), osteoclast number/bone area (Noc/BA), osteoblast number/bone perimeter (Nob/BPm) and osteoblast number/bone area (Nob/BA) were determined in trabecular bone of the metaphysis. The terminology and units used are those recommended by the Histomorphometry Nomenclature Committee of the American Society for Bone and Mineral Research [40]. Dynamic histomorphomtery was done on transverse cryosections through the mid-diaphysis of each tibiae previously labelled with calcein. Sections were cut at 15 μm using the CryoJane tape transfer system (Instrumedics, Hackensack, NJ) as previously described [41]. The sections were imaged with a Zeiss LSM 5 Pascal confocal microscope and the mineral apposition rate (MAR) was estimated as the distance between the two labels measured at equidistant points along the perimeter of the cortex and averaged for each bone.

2.7 Colony forming units (CFUs)

Bone marrow cells were harvested from tibiae of 6 WT and 6 *Phospho1*$^{-/-}$ 4 week old male mice and resuspended in α-MEM medium containing 10% FBS, gentamycin (50μg/ml), 100μM ascorbate-2-phosphate and 10 nM dexamethasone. Cells were plated in a six well plate at a density of $2x10^6$ cells/well. Medium was changed after 5 days and then every 3 days. Cells were maintained in culture for 15 days, reacted for alkaline phosphatase activity and then the number of colonies formed was counted.

2.8 Biochemical markers of bone turnover

Bone formation and resorption markers were measured in serum from 4-week old WT (n=16) and *Phospho1*$^{-/-}$ (n=14) male mice using Rat/Mouse Procollagen type I N-terminal propeptide (PINP, intra- and inter-assay variation, CV, is 5.0–7.4% and 8.0–9.2%, respectively) and C-terminal telopeptides of type I collagen (RatLaps™, intra- and inter-assay variation, CV, is 5.6–9% and 10.5–14.8%, respectively) enzyme immunoassays (IDS, Boldon, UK), respectively and run according to the manufacturer's instructions.

2.9 Statistics

All data were checked for normality and equal variance. Unless stated otherwise, normally distributed data were analyzed using Student's *t*-test, while the non-parametric data were analyzed using a Mann-Whitney Rank Sum test. All analyses were conducted with SigmaStat software (v 11.0).

3 Results

3.1 The long bones of *Phospho1*$^{-/-}$ mice do not fracture during 3-point bending

Previous analysis of *Phospho1*$^{-/-}$ mice revealed reduced accumulation of osteoid in the long bones, reduced ash mineral content and reduced bone mineral density (BMD) of cortical bone [29]. Therefore, the consequence of this hypomineralized matrix on the biomechanical properties of *Phospho1*$^{-/-}$ bones was first determined. Three-point bending analysis indicated that the failure load was not statistically different in the tibia (P=0.85) and femur (P=0.60) between the WT and *Phospho1*$^{-/-}$ mice (Fig. 1a-d and Suppl. table 1). The maximum stiffness and yield of the tibia and femur could not be determined in all bones because the maximum gradient of the load - extension curve occurred at the origin and, therefore, there was no yield point according to our definition of yield. A function fitted on the linear region of the load-extension curve also showed no significant differences between the slope of the WT and *Phospho1*$^{-/-}$ tibiae (P=0.744) and femora (P=0.516). Despite the fact that there were no significant differences in the load extension curve until the failure

point, *Phospho1*$^{-/-}$ bones did not fracture upon bending and tests were terminated when the ends of the bone touched the central anvil and the load increased (Figs. 1c and 1d). The rise at the end of the *Phospho1*$^{-/-}$ curves is due to impingement on the loading anvils. After testing, *Phospho1*$^{-/-}$ bones were very pliable and could be returned to their original shape, and bent again, still without breaking (Fig. 1e). This was in contrast to the tibia and femur from the WT mice where fracture did occur in the majority of the bones tested (Figs. 1a and 1b and Suppl. table 1). Some WT bones did not show a fracture point on the load-extension curve, due to the diaphysis contacting the jig, however, when removed from the testing machine the bones were fractured. This increased capability for "plastic" deformation recorded in the *Phospho1*$^{-/-}$ bones is consistent with the greenstick fractures observed in the soft bones of the these young mice [29].

3.2 Elasticity and hardness are decreased, while viscosity is increased in *Phospho1*$^{-/-}$ bones as determined by nanoindentation

The analysis of the mechanical behaviour of the whole bone as assessed by 3-point bending was limited by the inability to determine both maximum stiffness and yield and its inherent limitation to determine only extrinsic properties. To determine the properties at the tissue/ECM level we next assessed the intrinsic mechanical properties (Table 1) of the WT and *Phospho1*$^{-/-}$ femur and tibia by nanoindentation. In comparison to measurements in WT bones, dynamic testing of the *Phospho1*$^{-/-}$ tibia indicated that the complex, storage and loss moduli and plasticity index were significantly decreased by 13.5%, 13.3%, 7.3% ($P<0.005$) and 2.6% ($P<0.05$), respectively, while the loss tangent increased 7.8% ($P<0.05$). A quasistatic loading test showed a significant decrease only in the elastic modulus of 10.7% ($P<0.05$) within the tibia. Analysis for the curve fitting showed an increase in creep amplitude A, from 0.032 to 0.036 (12.5%) and decreased early creep strain rate B, from 0.23 to 0.20 (13%) also within the tibia. The response in femora was similar to tibiae but significant differences were limited due to a decreased storage modulus (7.3%, $p<0.05$) between WT and *Phospho1*$^{-/-}$ mice (Table 1). These data indicate that the tibiae of the *Phospho1*$^{-/-}$ mice are softer, more viscous but less elastic and cannot store strain energy as efficiently as the WT mice. The differences observed between femora and tibiae are not uncommon and are maybe due to altered loading of the individual long bones of the mouse hind leg.

3.3 Material properties of *Phospho1*$^{-/-}$ bones are altered

Bone strength and stiffness are determined by the characteristics of the bone ECM, the mineral which is formed within it and interactions between the mineral and components of the matrix. In this way it behaves like a composite material [42]. We therefore next examined the femora and tibiae of WT and *Phospho1*$^{-/-}$ mice by Raman microscopy to determine the composition of the inorganic and organic phases of these bones (Fig. 2). Tibial bone from *Phospho1*$^{-/-}$ mice had significantly reduced mineral to matrix (Fig. 2a) and carbonate to phosphate (Fig. 2b) ratios but an increased relative amount of HPO_4^- (Fig 2c) compared with WT animals. Similar trends were seen in the femur although only carbonate/phosphate reached significance. There was no difference in mineral crystallinity, as determined by the width of the phosphate ν_1 peak, between the two phenotypes, (Fig. 2d). These results suggest the ECM of the *Phospho1*$^{-/-}$ bones was less mineralized and the mineral itself had a lower concentration of carbonate but more HPO_4^-.

Collagen fibers within bone are stabilized predominantly by reducible, immature crosslinks (i.e. measured as their reduced forms hydroxylysinonorleucine (HLNL) and dehydroxylysinonorleucine (DHLNL)) and non-reducible mature crosslinks (i.e. pyridinoline, (PYD) and deoxypyridinoline (DPD)), both of which contribute to the mechanical strength of bone [43]. As expected the young bones analyzed in this study had a

greater amount of total immature than mature cross-links. There were no differences between WT and *Phospho1*$^{-/-}$ mice in the total amount of immature cross-links in either the tibia or the femur and in the total amount of mature cross-links in the femur, although this just reached significance in the tibia (Table 2). There were, however significantly higher DHLNL:HLNL and PYD:DPD ratios in both the tibia and femur of the *Phospho1*$^{-/-}$ mice compared with WT bones (Table 2). The *Phospho1*$^{-/-}$ femur had a greater collagen content (% dry weight) than the WT femur (P=0.008), which resulted in a lower calcium/collagen ratio (P=0.008). This pattern was not observed in the tibia (Table 2).

3.4 *Phospho1*$^{-/-}$ mice have increased cortical bone turnover

In addition to structural and material properties of bone, bone strength and mineralization status are influenced by the rates of bone formation and bone resorption [44]. The number of osteoblasts and osteoclasts per bone perimeter (Nob/BPm, Noc/BPm) were similar in both WT and *Phospho1*$^{-/-}$ bones as were the number of osteoblasts and osteoclasts per bone area (Nob/BA, Noc/BA) as measured by histomorphometrical analysis of the trabecular compartment (Table 3). Calcein labelling of the mid diaphysis of the tibia showed no significant differences in mineral apposition rate (MAR) between WT and *Phospho1*$^{-/-}$ bones (Fig. 3a). *Phospho1*$^{-/-}$ tibiae were, however, marked by extensive cortical bone turnover/callus formation regions (Fig. 3b). Five of the 7 *Phospho1*$^{-/-}$ samples examined had extensive areas of unorganized “woven-like” bone tissue whereas only 1 of the 6 WT samples examined (Fig. 3c) showed a similar feature and may be indicative of a repair mechanism for greenstick or fatigue fractures. Consistent with this increased cortical bone turnover there were significantly elevated levels of serum bone formation (propeptide of type I collagen, PINP) and bone resorption (C-terminal telopeptides of type I collagen, RatLaps™) markers in the *Phospho1*$^{-/-}$ mice (P<0.001, Fig. 4). In vitro, WT and *Phospho1*$^{-/-}$ bone marrow stromal cell cultures produced similar numbers of alkaline phosphatase positive colony forming units (CFUs, pre- osteoblasts; CFU-AP+, WT 29.1 ± 0.17, *Phospho1*$^{-/-}$ 23.7 ± 6.99), suggesting that osteoblast differentiation potential in *Phospho1*$^{-/-}$ bones was normal.

4 Discussion

The contribution to bone quality of the skeletal-specific phosphatase, PHOSPHO1, is now emerging [27,29]. When identified over 10 years ago we hypothesized that PHOSPHO1 was involved in the generation of cytosolic Pi to maintain a Pi/PPi ratio permissive for matrix mineralization [22]. This premise has been upheld in this and other recent studies in which the ablation of PHOSPHO1 function in mice results in a number of skeletal abnormalities that include decreased BMD, osteoidosis and altered geometry and microarchitecture [29] of the skeletal ECM. It is likely that the altered bone shape and bone architecture reflect compensatory changes for the lower mineralization status of the *Phospho1*$^{-/-}$ bones. The previously observed stockier bones of *Phospho1*$^{-/-}$ mice [29] provide greater resistance to bending and torsion loads [45] whereas more trabeculae provide greater support to the weaker (thinner and more porous) cortex [46–47]. Nevertheless despite these compensatory structural changes greenstick spontaneous fractures are observed in juvenile *Phospho1*$^{-/-}$ mice, as early as day 1, possibly indicating that other determinants of bone strength such as intrinsic material properties and modelling rates are altered [29]. Moreover, we have an incomplete picture of how reduced BMD and changes in structural and material integrity affect the mechanical properties of bone.

Biomechanical analysis of the cortical bone by 3-point bending indicated that, in comparison with WT bones, the tibia and femur of *Phospho1*$^{-/-}$ mice displayed plastic deformation rather than a clean fracture. While this is probably due to the low mineralization status, the young age of the mice may also contribute. The capacity for greater plastic deformation

recorded in the *Phospho1*$^{-/-}$ bones is similar to that seen in the undermineralized bones with osteomalacia, which are known to be tougher and more ductile [48–49] than healthy bones. Intrinsic properties of *Phospho1*$^{-/-}$ ECM behaved as expected based on previously observed patterns, where a less mineralized matrix is lower in elasticity and softer in nature [34–35,50], as shown by a smaller storage modulus and larger loss modulus. Bone is a viscoelastic material where the viscous part of the applied load (energy) is lost as it is absorbed within ECM, causing permanent changes in bone shape. The elastic part of the applied load, although also stored within the ECM, is released and the original morphology is restored upon removal of loading. Thus, the *Phospho1*$^{-/-}$ bone tissue is more viscous because it exhibits higher ductility as more energy is used to cause viscous deformations. The simplest explanation for the increased plasticity of the *Phospho1*$^{-/-}$ bones is the reduction in the mineral component of the *Phospho1*$^{-/-}$ ECM [34,50]. This is in agreement with our working hypothesis that PHOSPHO1 is a skeletal-specific phosphatase liberating Pi for HA formation and is consistent with our previous report [29] of reduced ash and BMD in *Phospho1*$^{-/-}$ bones and also with the lower phosphate to matrix ratio of *Phospho1*$^{-/-}$ bones identified by Raman microscopy in the present study. However, bone strength and mechanical properties are also influenced by the characteristics of the bone ECM in which the mineral is embedded and the crystallinity of the mineral itself. The way ECM and mineral interact is also important for the strength of the composite material [42]. With ageing, the number of carbonate substitutions in place of phosphate or hydroxyl groups is known to increase and the relative amount of acid-phosphate (HPO_4^-) to decrease [51]. The Raman data, therefore, suggest a younger, less mature matrix, more able to deform without fracture [52]. A younger matrix is consistent with the increased amount of markers for bone formation and resorption, indicating an increase in bone turnover.

The major organic component of the bone ECM is collagen type I, which is assembled into both fibrils and fibres stabilized by cross-links. Collagen cross-links contribute to the mechanical strength of the bone by influencing both fibril strength and the size and shape of the regions between the collagen molecules available for crystal deposition [53–55]. However, as the concentration of mature (PYD and DPD) and immature (DHLNL and HLNL) cross-links were similar in the WT and *Phospho1*$^{-/-}$ bones it is unlikely that the altered mechanical properties of the *Phospho1*$^{-/-}$ bones are due to fewer cross-links. The most significant alterations in the crosslink profile between the WT and *Phospho1*$^{-/-}$ bones were the DHLNL:HLNL and PYD:DPD ratios which are known to influence human trabecular bone quality [56]. The altered ratios may reflect different degrees of hydroxylation of specific helical lysine residues by the enzyme lysyl hydroxylase 1 [56–57], which would lead to a greater proportion of hydroxylysine residues relative to lysine residues adjacent to the telopeptide aldehydes. Alternatively, it has previously been reported that the lysyl hydroxylation of tendon collagen type I was reduced on the mineralization of the tendon suggesting that the low amounts of PYD, and hence lower PYD:DPD ratio maybe be associated with the mineralization process itself [58]. Therefore it is possible that the higher PYD:DPD ratio observed in the *Phospho1*$^{-/-}$ bones may be a consequence of the hypomineralization of these bones.

As both osteoclast and osteoblast numbers within the trabecular compartment and the osteoblast differentiation potential (pre- osteoblasts; CFU-AP+) of *Phospho1*$^{-/-}$ mice were normal it is unlikely that the increased levels of formation and resorption markers quantified in the *Phospho1*$^{-/-}$ serum samples are a result of increased cell number/activity or osteoblast differentiation potential. It is more plausible that the increased serum bone markers in *Phospho1*$^{-/-}$ mice are a result of fracture repair which is secondary to greenstick fractures that occur in the hypomineralized bone of the *Phospho1* $^{-/-}$ mice. [29]. Furthermore the viscoplastic damage noted in the *Phospho1*$^{-/-}$ bones is likely to be sensed by the osteocyte [59], triggering bone remodelling and the generation of fracture calluses in

the *Phospho1*$^{-/-}$ mice in a similar manner to that reported in greenstick fractures of children [29,60]. Alternatively the increased PINP and RatLaps™ may reflect an attempt to model into a mechanically competent bone capable of withstanding physiological load.

In conclusion we have shown in this study that the absence of PHOSPHO1 results in a lower accumulation of mineral in bones. This leads to differences in bone mineral quantity and composition and, as a result, the bone is more deformable. This provides an explanation for the greenstick fractures and the skeletal deformations observed in these mice. We hypothesize that the poorer quality of the mineral and the lower ECM mineralization induces an increase in bone turnover as the bone attempts to repair and/or to model itself to create a mechanically competent bone.

Supplementary Material

Refer to Web version on PubMed Central for supplementary material.

Acknowledgments

This work was supported in part by grants DE12889, AR47908 and AR53102 from the National Institutes of Health, USA and Institute Strategic Programme Grant funding from the Biotechnology and Biological Sciences Research Council (BBSRC), UK. The authors are grateful to Ms. Jessica Groos for the maintenance of the mouse colonies at the Burnham Institute for Medical Research and Miss Elaine Seawright and Mr. Juha-Pekka Miettinen for technical help during the completion of these studies.

References

1. Golub EE. Role of matrix vesicles in biomineralization. Biochim Biophys Acta. 2009; 1790:1592–1598. [PubMed: 19786074]
2. Anderson HC, Garimella R, Tague SE. The role of matrix vesicles in growth plate development and biomineralization. Front Biosci. 2005; 10:822–837. [PubMed: 15569622]
3. Wu LN, Genge BR, Kang MW, Arsenault AL, Wuthier RE. Changes in phospholipids extractability and composition accompany mineralization of chicken growth plate cartilage matrix vesicles. J Biol Chem. 2002; 277:5126–5133. [PubMed: 11714705]
4. Suzuki A, Ghayor C, Guicheux J, Magne D, Quillard S, Kakita A, Ono Y, Miura Y, Oiso Y, Itoh M, Caverzasio J. Enhanced expression of the inorganic phosphate transporter Pit-1 is involved in BMP-2-induced matrix mineralization in osteoblast-like cells. J Bone Miner Res. 2006; 21:674–683. [PubMed: 16734382]
5. Polewski MD, Johnson KA, Foster M, Millan JL, Terkeltaub R. Inorganic pyrophosphatase induces type I collagen in osteoblasts. Bone. 2010; 46:81–90. [PubMed: 19733704]
6. Kim HJ, Kirsch T. Collagen/annexin V interactions regulate chondrocyte mineralization. J Biol Chem. 2008; 283:10310–10317. [PubMed: 18281278]
7. Harmey D, Hessle L, Narisawa S, Johnson KA, Terkeltaub R, Millan JL. Concerted regulation of inorganic pyrophosphate and osteopontin by akp2, enpp1, and ank: an integrated model of the pathogenesis of mineralization disorders. Am J Pathol. 2004; 164:1199–1209. [PubMed: 15039209]
8. Meyer JL. Can biological calcification occur in the presence of pyrophosphate? Arch Biochem Biophys. 1984; 231:1–8. [PubMed: 6326671]
9. Moss DW, Eaton RH, Smith JK, Whitby LG. Association of inorganic-pyrophosphatase activity with human alkaline-phosphatase preparations. Biochem J. 1967; 102:53–57. [PubMed: 6030299]
10. Majeska RJ, Wuthier RE. Studies on matrix vesicles isolated from chick epiphyseal cartilage. Association of pyrophosphatase and ATPase activities with alkaline phosphatase. Biochim Biophys Acta. 1975; 391:51–60. [PubMed: 237558]
11. Hessle L, Johnson KA, Anderson HC, Narisawa S, Sali A, Goding JW, Terkeltaub R, Millan JL. Tissue-nonspecific alkaline phosphatase and plasma cell membrane glycoprotein-1 are central antagonistic regulators of bone mineralization. Proc Natl Acad Sci U S A. 2002; 99:9445–9449. [PubMed: 12082181]

12. Murshed M, Harmey D, Millan JL, McKee MD, Karsenty G. Unique coexpression in osteoblasts of broadly expressed genes accounts for the spatial restriction of ECM mineralization to bone. Genes Dev. 2005; 19:1093–1104. [PubMed: 15833911]

13. Terkeltaub R, Rosenbach M, Fong F, Goding J. Causal link between nucleotide pyrophosphohydrolase overactivity and increased intracellular inorganic pyrophosphate generation demonstrated by transfection of cultured fibroblasts and osteoblasts with plasma cell membrane glycoprotein-1. Relevance to calcium pyrophosphate dihydrate deposition disease. Arthritis Rheum. 1994; 37:934–941. [PubMed: 8003067]

14. Hakim FT, Cranley R, Brown KS, Eanes ED, Harne L, Oppenheim JJ. Hereditary joint disorder in progressive ankylosis (ank/ank) mice. I. Association of calcium hydroxyapatite deposition with inflammatory arthropathy. Arthritis Rheum. 1984; 27:1411–1420. [PubMed: 6095872]

15. Ho AM, Johnson MD, Kingsley DM. Role of the mouse ank gene in control of tissue calcification and arthritis. Science. 2000; 289:265–270. [PubMed: 10894769]

16. Ciancaglini P, Yadav MC, Simao AM, Narisawa S, Pizauro JM, Farquharson C, Hoylaerts MF, Millan JL. Kinetic analysis of substrate utilization by native and TNAP-, NPP1-, or PHOSPHO1-deficient matrix vesicles. J Bone Miner Res. 2010; 25:716–723. [PubMed: 19874193]

17. Whyte, MP. Hypophosphatasia: Nature's window on alkaline phosphatase function in humans. In: Bilezikian, JP.; Raisz, LG.; Martin, TJ., editors. Principles of bone biology. 3rd ed.. San Diego, California: Academic Press; 2008. p. 1573-1598.

18. Narisawa S, Frohlander N, Millan JL. Inactivation of two mouse alkaline phosphatase genes and establishment of a model of infantile hypophosphatasia. Dev Dyn. 1997; 208:432–446. [PubMed: 9056646]

19. Fedde KN, Blair L, Silverstein J, Coburn SP, Ryan LM, Weinstein RS, Waymire K, Narisawa S, Millan JL, MacGregor GR, Whyte MP. Alkaline phosphatase knock-out mice recapitulate the metabolic and skeletal defects of infantile hypophosphatasia. J Bone Miner Res. 1999; 14:2015–2026. [PubMed: 10620060]

20. Anderson HC, Hsu HH, Morris DC, Fedde KN, Whyte MP. Matrix vesicles in osteomalacic hypophosphatasia bone contain apatite-like mineral crystals. Am J Pathol. 1997; 151:1555–1561. [PubMed: 9403706]

21. Anderson HC, Sipe JB, Hessle L, Dhanyamraju R, Atti E, Camacho NP, Millan JL. Impaired calcification around matrix vesicles of growth plate and bone in alkaline phosphatase-deficient mice. Am J Pathol. 2004; 164:841–847. [PubMed: 14982838]

22. Houston B, Seawright E, Jefferies D, Hoogland E, Lester D, Whitehead C, Farquharson C. Identification and cloning of a novel phosphatase expressed at high levels in differentiating growth plate chondrocytes. Biochim Biophys Acta. 1999; 1448:500–506. [PubMed: 9990301]

23. Stewart AJ, Schmid R, Blindauer CA, Paisey SJ, Farquharson C. Comparative modelling of human PHOSPHO1 reveals a new group of phosphatases within the haloacid dehalogenase superfamily. Protein Eng. 2003; 16:889–895. [PubMed: 14983068]

24. Stewart AJ, Roberts SJ, Seawright E, Davey MG, Fleming RH, Farquharson C. The presence of PHOSPHO1 in matrix vesicles and its developmental expression prior to skeletal mineralization. Bone. 2006; 39:1000–1007. [PubMed: 16837257]

25. Roberts S, Narisawa S, Harmey D, Millan JL, Farquharson C. Functional involvement of PHOSPHO1 in matrix vesicle-mediated skeletal mineralization. J Bone Miner Res. 2007; 22:617–627. [PubMed: 17227223]

26. Roberts SJ, Stewart AJ, Schmid R, Blindauer CA, Bond SR, Sadler PJ, Farquharson C. Probing the substrate specificities of human PHOSPHO1 and PHOSPHO2. Biochim Biophys Acta. 2005; 1752:73–82. [PubMed: 16054448]

27. Macrae VE, Davey MG, McTeir L, Narisawa S, Yadav MC, Millan JL, Farquharson C. Inhibition of PHOSPHO1 activity results in impaired skeletal mineralization during limb development of the chick. Bone. 2010; 46:1146–1155. [PubMed: 20053388]

28. Roberts SJ, Stewart AJ, Sadler PJ, Farquharson C. Human PHOSPHO1 exhibits high specific phosphoethanolamine and phosphocholine phosphatase activities. Biochem J. 2004; 382:59–65. [PubMed: 15175005]

29. Yadav MC, Simao AM, Narisawa S, Huesa C, McKee MD, Farquharson C, Millan JL. Loss of skeletal mineralization by the simultaneous ablation of PHOSPHO1 and alkaline phosphatase function - A unified model of the mechanisms of initiation of skeletal calcification. J Bone Miner Res. 2011 [Epub ahead of print].
30. Rawlinson SC, Murray DH, Mosley JR, Wright CD, Bredl JC, Saxon LK, Loveridge N, Leterrier C, Constantin P, Farquharson C, Pitsillides AA. Genetic selection for fast growth generates bone architecture characterised by enhanced periosteal expansion and limited consolidation of the cortices but a diminution in the early responses to mechanical loading. Bone. 2009; 45:357–366. [PubMed: 19409517]
31. Aspden RM. Mechanical testing of bone ex vivo. Methods Mol Med. 2003; 80:369–379. [PubMed: 12728732]
32. Goodyear SR, Gibson IR, Skakle JM, Wells RP, Aspden RM. A comparison of cortical and trabecular bone from C57 Black 6 mice using Raman spectroscopy. Bone. 2009; 44:899–907. [PubMed: 19284975]
33. de Mul FF, Hottenhuis MH, Bouter P, Greve J, Arends J, ten Bosch JJ. Micro-Raman line broadening in synthetic carbonated hydroxyapatite. J Dent Res. 1986; 65:437–440. [PubMed: 3007591]
34. Finnila MA, Zioupos P, Herlin M, Miettinen HM, Simanainen U, Hakansson H, Tuukkanen J, Viluksela M, Jamsa T. Effects of 2,3,7,8-tetrachlorodibenzo-p-dioxin exposure on bone material properties. J Biomech. 2010; 43:1097–1103. [PubMed: 20132933]
35. Ferguson VL. Deformation partitioning provides insight into elastic, plastic, and viscous contributions to bone material behavior. J Mech Behav Biomed Mater. 2009; 2:364–374. [PubMed: 19627843]
36. Lewis G, Jeffry SN. The use of nanoindentation for characterizing the properties of mineralizing hard tissues: state-of-the art review. M Biomed Mater Res B Appl Biomater. 2008; 87:286–301.
37. Black D, Duncan A, Robins SP. Quantitative analysis of the pyridinium crosslinks of collagen in urine using ion-paired reversed-phase high-performance liquid chromatography. Anal Biochem. 1988; 169:197–203. [PubMed: 3369682]
38. Gineyts E, Borel O, Chapurlat R, Garnero P. Quantification of immature and mature collagen crosslinks by liquid chromatography-electrospray ionization mass spectrometry in connective tissues. J Chromatogr B Analyt Technol Biomed Life Sci. 2010; 878:1449–1454.
39. Firschein HE, Shill JP. The determination of total hydroxyproline in urine and bone extracts. Anal Biochem. 1966; 14:296–304. [PubMed: 5939867]
40. Parfitt AM. Bone histomorphometry: standardization of nomenclature, symbols and units (summary of proposed system). Bone. 1988; 9:67–69. [PubMed: 3377921]
41. Owen HC, Roberts SJ, Ahmed SF, Farquharson C. Dexamethasone-induced expression of the glucocorticoid response gene lipocalin 2 in chondrocytes. Am J Physiol Endocrinol Metab. 2008; 294:E1023–E1034. [PubMed: 18381927]
42. Landis WJ. The strength of a calcified tissue depends in part on the molecular structure and organization of its constituent mineral crystals in their organic matrix. Bone. 1995; 16:533–544. [PubMed: 7654469]
43. Knott L, Bailey AJ. Collagen cross-links in mineralizing tissues: a review of their chemistry, function, and clinical relevance. Bone. 1998; 22:181–187. [PubMed: 9514209]
44. Felsenberg D, Boonen S. The bone quality framework: determinants of bone strength and their interrelationships, and implications for osteoporosis management. Clin Ther. 2005; 27:1–11. [PubMed: 15763602]
45. Bouxsein ML. Mechanisms of osteoporosis therapy: a bone strength perspective. Clin Cornerstone. 2003 Suppl 2:S13–S21. [PubMed: 15035555]
46. Kleerekoper M, Villanueva AR, Stanciu J, Rao DS, Parfitt AM. The role of three-dimensional trabecular microstructure in the pathogenesis of vertebral compression fractures. Calcif Tissue Int. 1985; 37:594–597. [PubMed: 3937580]
47. Weinstein RS, Hutson MS. Decreased trabecular width and increased trabecular spacing contribute to bone loss with aging. Bone. 1987; 8:137–142. [PubMed: 3606904]

48. Currey JD. Physical characteristics affecting the tensile failure properties of compact bone. J Biomech. 1990; 23:837–844. [PubMed: 2384495]

49. Turner CH. Biomechanics of bone: determinants of skeletal fragility and bone quality. Osteoporos Int. 2002; 13:97–104. [PubMed: 11905527]

50. Zioupos P. In vivo fatigue microcracks in human bone: material properties of the surrounding bone matrix. Eur J Morphol. 2005; 42:31–41. [PubMed: 16123022]

51. Pellegrino ED, Biltz RM. Mineralization in the chick embryo. I. Monohydrogen phosphate and carbonate relationships during maturation of the bone crystal complex. Calcif Tissue Res. 1972; 10:128–135. [PubMed: 4343465]

52. Akkus O, Adar F, Schaffler MB. Age-related changes in physicochemical properties of mineral crystals are related to impaired mechanical function of cortical bone. Bone. 2004; 34:443–453. [PubMed: 15003792]

53. Lees S, Eyre DR, Barnard SM. BAPN dose dependence of mature crosslinking in bone matrix collagen of rabbit compact bone: corresponding variation of sonic velocity and equatorial diffraction spacing. Connect Tissue Res. 1990; 24:95–105. [PubMed: 2354637]

54. Oxlund H, Barckman M, Ortoft G, Andreassen TT. Reduced concentrations of collagen cross-links are associated with reduced strength of bone. Bone. 1995; 17:365S–371S. [PubMed: 8579939]

55. Follet H, Boivin G, Rumelhart C, Meunier PJ. The degree of mineralization is a determinant of bone strength: a study on human calcanei. Bone. 2004; 34:783–789. [PubMed: 15121009]

56. Banse X, Sims TJ, Bailey AJ. Mechanical properties of adult vertebral cancellous bone: correlation with collagen intermolecular cross-links. J Bone Miner Res. 2002; 17:1621–1628. [PubMed: 12211432]

57. Tasker PN, Macdonald H, Fraser WD, Reid DM, Ralston SH, Albagha OM. Association of PLOD1 polymorphisms with bone mineral density in a population-based study of women from the UK. Osteoporos Int. 2006; 17:1078–1085. [PubMed: 16758144]

58. Knott L, Tarlton JF, Bailey AJ. Chemistry of collagen cross-linking: biochemical changes in collagen during the partial mineralization of turkey leg tendon. Biochem J. 1997; 322(Pt 2):535–542. [PubMed: 9065774]

59. Burger EH, Klein-Nulend J, van der Plas A, Nijweide PJ. Function of osteocytes in bone--their role in mechanotransduction. J Nutr. 1995; 125:2020S–2023S. [PubMed: 7602386]

60. Todd TW, Iler DH. The Phenomena of Early Stages in Bone Repair. Ann Surg. 1927; 86:715–736. [PubMed: 17865776]

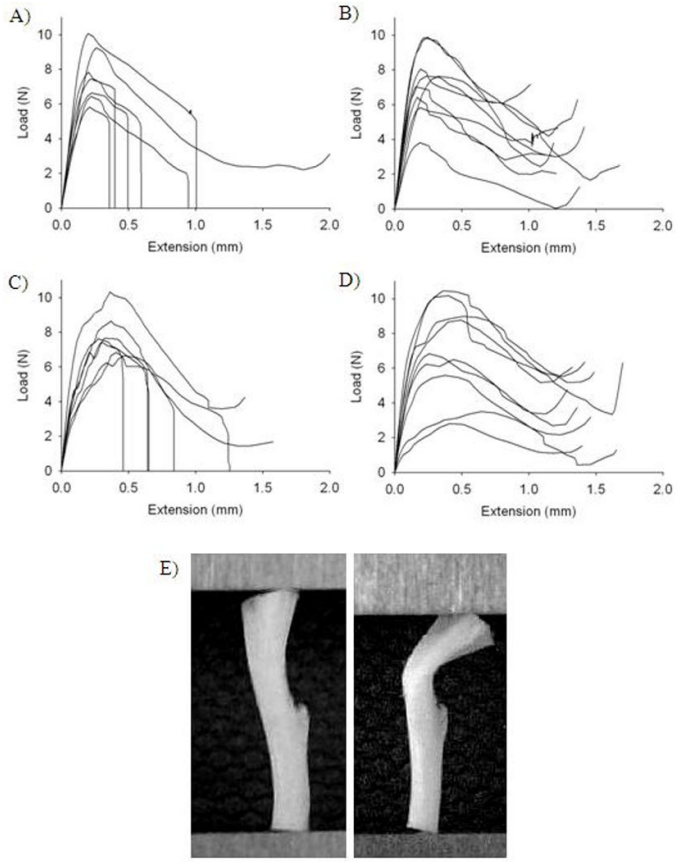

Figure 1.

Three point bending load vs extension graphs on 7 WT and 9 *Phospho1*$^{-/-}$ tibiae and femora: A) WT tibia, B) *Phospho1*$^{-/-}$ tibia, C) WT femur and D) *Phospho1*$^{-/-}$ femur. E) Representative images of the resilience of a *Phospho1*$^{-/-}$ tibia after three point bending test. A *Phospho1*$^{-/-}$ tibia was straightened after three point bending (left image) and bent again using callipers (right image).

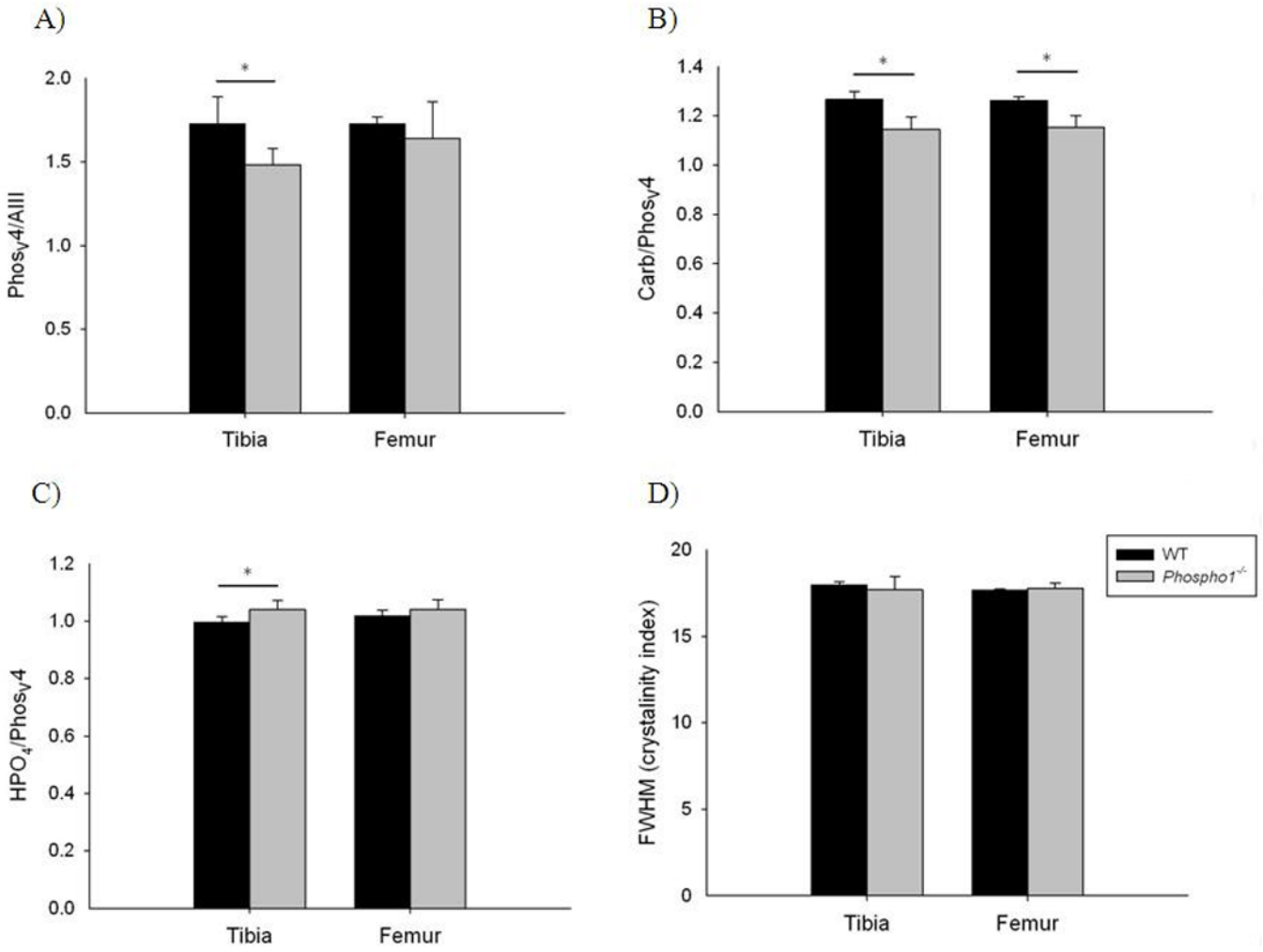

Figure 2.

Measurements of material composition on WT and *Phospho*1$^{-/-}$ cortical bone with Raman microscopy. A) Phosphate to matrix ratio, B) Carbonate to phosphate ratio, C) Phosphate to hydrogen phosphate ratio and D) crystallinity. N=5 (WT and *Phospho*1$^{-/-}$). Data is shown as mean ± SD. * P<0.05.

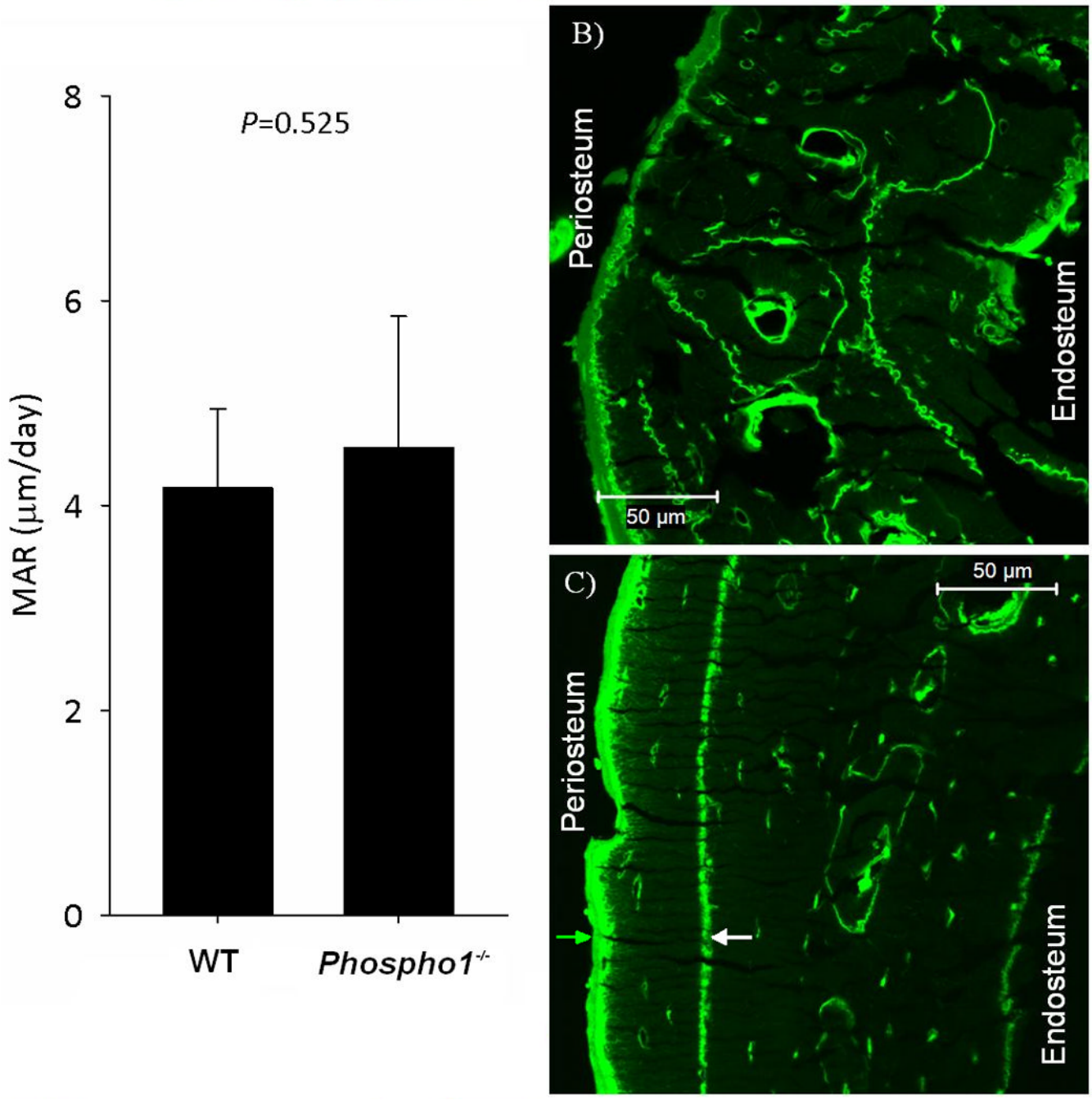

Figure 3.

Representative observations by dynamic bone histomorphometry in the mid-diaphyses of WT (N=6) and *Phospho1*$^{-/-}$ (N=7) tibiae. A) MAR was similar between WT and *Phospho1*$^{-/-}$ bones. B) Representative area of callus formation observed in a cortical bone cross-section of the *Phospho1*$^{-/-}$ tibia. Unorganized woven-like tissue was frequently noted in the anterior and posterior regions of the tibial cortex. C) Typical double labelling in WT tibia cortical bone cross-section indicative of bone growth.

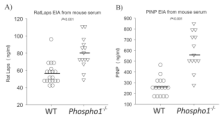

Figure 4.

Representation of bone turnover markers present in WT (N=16) and *Phospho1*$^{-/-}$ (N=14) mice serum as measured with enzyme immunoassays. A) Bone resorption marker RatLaps™. B) Bone formation marker PINP.

Table 1

Measurements of mechanical properties at the tissue level by nanoindentation on WT and Phospho1$^{-/-}$ cortical fragments of tibiae and femora. Measurements: Complex modulus (E_C), Storage (E_{Stor}), loss (E_{Loss}) modulus, phase difference (δ), plasticity Index (I_p), both static (H_S) and dynamic (H_D) hardness, Elastic modulus (E), overall creep amplitude (A_{Creep}) and early creep strain (B_{Creep}).

	Tibia		**Femur**	
Dynamic loading	**WT**	***Phospho1*$^{-/-}$**	**WT**	***Phospho1*$^{-/-}$**
E_C (GPa)	20.8 ± 1.3^b	18.0 ± 1.3	22.0 ± 1.9	20.4 ± 1.3
E_{Stor} (GPa)	23.3 ± 1.4^b	20.2 ± 1.4	24.6 ± 2.0^b	22.8 ± 1.5
E_{Loss} (GPa)	1.79 ± 0.04^b	1.66 ± 0.08	1.73 ± 0.08	1.64 ± 0.06
δ	0.077 ± 0.003 ^{a}	0.083 ± 0.003	0.071 ± 0.003	0.073 ± 0.005
H_S(GPa)	0.79 ± 0.07^a	0.70 ± 0.05	0.91 ± 0.10	0.84 ± 0.08
I_p	0.78 ± 0.01^a	0.76 ± 0.01	0.77 ± 0.00	0.77 ± 0.01
Quasistatic loading				
E (GPa)	20.5 ± 1.4^a	18.3 ± 1.9	21.1 ± 1.4	20.3 ± 1.9
H_D(GPa)	0.59 ± 0.04	0.56 ± 0.06	0.72 ± 0.09	0.66 ± 0.07
A_{Creep}	0.032 ± 0.011	0.036 ± 0.022	0.023 ± 0.002	0.025 ± 0.002
B_{Creep}	0.23 ± 0.08	0.20 ± 0.08	0.29 ± 0.03	0.28 ± 0.02

^{a} $P<0.05$;

^{b} $P<0.01$

Table 2

Measurements of collagen cross links in *Phospho*1$^{-/-}$ and WT mice cortical bone from tibiae and femora. Data are shown as mean ± SD unless distribution was not normal, in which case the median is shown. Abbreviations: Calcium (Ca), pyridinoline (PYD), deoxypyridinoline (DPD), dihydroxylysinonorleucine (DHLNL) and hydroxylysinonorleucine (HLNL),

Tibia	**WT**	***Phospho1*$^{-/-}$**	***P value***
Collagen	27.4	28.1	0.95
DHLNL	1.233 ± 0.15	1.352 ± 0.12	0.11
HLNL	0.202	0.187	0.029
Total reducible	1.44 ± 0.17	1.55 ± 0.13	0.21
DHLNL:HLNL	5.90 ± 0.49	7.48 ± 0.53	0.001
PYD	0.0329 ± 0.0030	0.0367 ± 0.003	0.026
DPD	0.0214 ± 0.0038	0.0167 ± 0.002	0.012
Total non-reducible	0.0664 ± 0.0077	0.0569 ± 0.009	0.049
PYD:DPD	1.56 ± 0.18	2.18 ± 0.31	0.0004
Collagen (% dry weight)	31.7 ± 7.6	29.0 ± 5.7	0.60
Ca/dry weight (μmol/mg)	5.88 ± 1.5	6.04 ± 0.95	0.90
Ca/collagen (μmol/nmol	6.00 ± 2.4	6.57 ± 1.6	0.81
Femur	WT	*Phospho1*$^{-/-}$	*P* value
Collagen	22.20 ± 1.6	26.4 ± 2.9	0.008
DHLNL	1.49 ± 0.060	1.55 ± 0.19	0.43
HLNL	0.160	0.128	0.029
Total reducible	1.64 ± 0.060	1.69 ± 0.21	0.64
DHLNL:HLNL	9.36 ± 0.723	11.5 ± 1.5	0.008
PYD	0.0444 ± 0.0029	0.0416 ± 0.0051	0.26
DPD	0.0221 ± 0.0049	0.0153 ± 0.0042	0.013
Total non-reducible	0.0543 ± 0.0064	0.0559 ± 0.0042	0.72
PYD:DPD	2.08 ± 0.352	2.84 ± 0.53	0.009
Collagen (% dry weight)	22.2 ± 1.6	26.37 ± 2.9	0.008
Ca/dry weight (μmol/mg)	6.76 ± 0.36	6.034 ± 0.60	0.020
Ca/collagen (μmol/nmol)	9.19 ± 1.1	7.01 ± 1.5	0.008

Table 3

Measurements from static hystomorphometry. Abbreviations: Number of osteoclasts (Noc), number of osteoblasts (Nob), bone area (BA) and bone perimeter (BPm).

	WT	*Phospho1*$^{-/-}$
Noc/BA (μm^{-2})	0.00082 ± 0.00069	0.000874 ± 0.00040
Noc/BPm (μm^{-1})	0.00784 ± 0.0042	0.0112 ± 0.0018
Nob/BA (μm^{-2})	0.00365 ± 0.0017	0.00382 ± 0.0015
Nob/BPm (μm^{-1})	0.0348 ± 0.010	0.0464 ± 0.016